MISSOURI S&T

Missouri University of Science and Technology

Scholars' Mine

Mechanical and Aerospace Engineering Faculty Research & Creative Works

Mechanical and Aerospace Engineering

01 Feb 1989

Measured Spectra of the Hygroscopic Fraction of Atmospheric Aerosol Particles

Darryl J. Alofs
Missouri University of Science and Technology, dalofs@mst.edu

Donald E. Hagen
Missouri University of Science and Technology, hagen@mst.edu

Max B. Trueblood
Missouri University of Science and Technology, trueblud@mst.edu

Follow this and additional works at: https://scholarsmine.mst.edu/mec_aereng_facwork

Part of the Aerospace Engineering Commons, Chemistry Commons, and the Physics Commons

Measured Spectra of the Hygroscopic Fraction of Atmospheric Aerosol Particles

DARRYL J. ALOFS,* DONALD E. HAGEN† AND MAX B. TRUEBLOOD

Graduate Center for Cloud Physics Research, University of Missouri-Rolla, Rolla, Missouri

ABSTRACT

The relation between dry diameter (X_0) and critical supersaturation (S_c) for atmospheric submicron aerosol particles is investigated using a long term air sampling program at Rolla, Missouri. The particles are passed through an electrostatic aerosol size classifier, and then through an isothermal haze chamber. Results are reported in terms of an apparent volume fraction of soluble material, ϵ_v, defined such that for particles composed only of ammonium sulfate and water insoluble compounds, ϵ_v is the actual volume fraction of soluble material. The probability distribution of ϵ_v is found to be approximately Gaussian in the ϵ_v range 0.2 to 1.3. The mean ϵ_v is 0.5, for electrostatic aerosol classifier settings of 0.2, 0.3, and 0.4 μm diameter.

1. Introduction

This investigation concerns measurements of critical supersaturations (S_c) of atmospheric aerosol particles. The measurements are made after passing the atmospheric aerosol through an electrostatic aerosol classifier (EAC) set to pass either 0.2, 0.3, or 0.4 μm diameter particles. The air sampling was done at a small town (Rolla, Missouri) with the equipment running nearly 24 hours per day for about 100 days, with the sampling days spread quite uniformly through the four seasons of the year. Similar measurements were made by Fitzgerald et al. (1982) and by Fitzgerald and Hoppel (1984). Their measurements were for smaller particles and for shorter time periods at various geographic locations. Sekigawa (1983) reports similar measurements made 60 km Northeast of Tokyo.

Fitzgerald et al. (1982) rearrange equations by Hänel (1976) to obtain a convenient relation between the equilibrium diameter (X_e) of a hygroscopic particle and the saturation ratio (S_r) of the air-water vapor mixture surrounding it. The equation is:

$$S_r = \exp\left(\frac{2A}{X_e}\right)\exp\left(-\frac{B}{(X_e^3/X_0^3)-1}\right), \quad (1)$$

where A involves surface tension and temperature, X_0 is the dry diameter of the particle, and B is the following

---

* Also affiliated with Department of Mechanical and Aerospace Engineering, University of Missouri-Rolla.

† Also affiliated with Department of Physics, University of Missouri-Rolla.

Corresponding author address: Dr. Darryl J. Alofs, Graduate Center for Cloud Physics Research, University of Missouri, Rolla, Rolla, Missouri 65401.

dimensionless group of physical and chemical properties:

$$B = \rho_0\nu\phi\epsilon_m M_w/\rho_w M_s \quad (2a)$$

or

$$B = \rho_s\nu\phi\epsilon_v M_w/\rho_w M_s, \quad (2b)$$

where ρ_0 is the density of the particle in dry state, ν is the number of ions formed per molecule of solute, ϕ is the osmotic coefficient of the solution, ϵ_m is the mass fraction of soluble material, ϵ_v is the volume fraction of soluble material, ρ_s is the density of the soluble material, M_s is the mean molecular weight of the soluble material, M_w is the molecular weight of water, and ρ_w is the density of water.

The quantity B varies with X_e, mainly because of the osmotic coefficient, which is a function of the molality of the solution droplet. The value of B at the peak S_r is called B_c, and the value of B at very large X_e is called B^0. The corresponding values of ϕ are denoted ϕ_c and ϕ_0. Since the ϕ for a very dilute solution is unity, $\phi_0 = 1$.

If B is taken to be constant near the peak S_r for a given particle, the peak saturation ratio (equivalent to $S_c + 1$) can be found analytically. The result is:

$$S_c B_c^{1/2} X_0^{3/2} = C_1, \quad (3)$$

where the value of C_1 at 20 C is 0.003818 for S_c in percent and X_0 in μm. The above equation is given as Eq. 11 in Fitzgerald et al. (1982). In the paragraph following Eq. 11, Fitzgerald et al. (1982) adopt the approximation $B^0 = 1.1B_c$, which implies that $\phi_c = 1/1.1 = 0.9091$ for atmospheric particles in the regime of their measurements $(0.06~\mu\text{m} \leqslant X_0 \leqslant 0.16~\mu\text{m})$.

Hänel (1976) performed numerical computations to obtain S_c values using equations equivalent to (1).

Hänel's computations can be used to check the accuracy of (3). His computations are for 20 C, with ammonium sulfate as the soluble constituent and for X_0 in the range 0.02 to 20 μm. The values of ϵ_v, X_0, and S_c from Table X in Hänel (1976) can be used to make a plot of the parameter $S_c\epsilon_v^{1/2}X_0^{3/2}$ versus S_c. The result is Fig. 1. It can be seen from Fig. 1 that for $\epsilon_v \geq 0.01$ and $S_c \leq 0.1\%$ the parameter $S_c\epsilon_v^{1/2}X_0^{3/2}$ is nearly constant, having only a slight dependence on S_c, and showing virtual independence of ϵ_v. We fitted a polynomial to represent the dependence on S_c, and thus we represent the Hänel computations by the equation:

$$S_c\epsilon_v^{1/2}X_0^{3/2} = C_2(1 + \theta), \qquad (5)$$

where $C_2 = 0.00481$ and θ is given by the polynomial:

$$\theta = -0.038995 + 0.54701S_c$$
$$- 1.47612S_c^2 + 1.27811S_c^3. \quad (6)$$

The polynomial is accurate only for $S_c \leq 0.7\%$. For the range of the present investigation ($0.014\% < S_c < 0.10\%$) the value of θ increases monotonically from -0.032 to $+0.0022$. Since θ is small, Hänel's computations support the accuracy of (3). Also, if one takes $\theta = 0$ in (5), a comparison of (5) and (3) gives $\epsilon_v = 1.587B_c$.

We have chosen to represent our data in terms of "apparent" ϵ_v values calculated using (5). These apparent ϵ_v values equal the actual volume fraction of soluble material only if the soluble material is actually ammonium sulfate. Another possibility would have been to represent the data in terms of B_c or B^0 values. The reader who prefers B_c can convert using $\epsilon_v/B_c = 1.587$.

Fitzgerald et al. (1982) use a simple method to obtain mean B_c values from their measurements. Particular kinds of mean S_c and X_0 are defined. These are used in (3) to obtain mean B_c values. The accuracy of this type of approximation is intuitively expected to decrease as the spread of either X_0 or B_c increases.
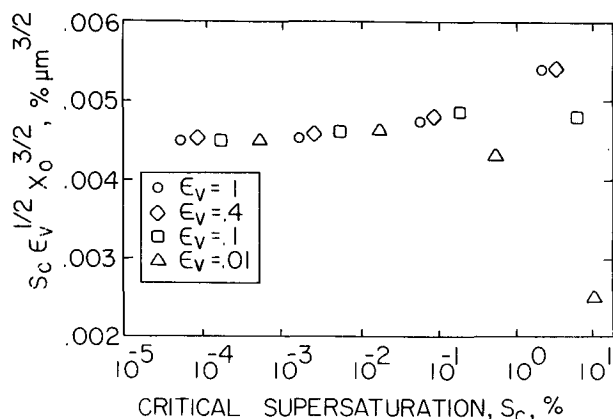
An innovative portion of this investigation has been developing an inversion method to obtain spectra of ϵ_v from the measured spectra of S_c. The inversion method is more rigorous than the simple method used by Fitzgerald et al. (1982). In addition to providing more accurate mean ϵ_v (or B_c) values, the inversion gives information about the spread of ϵ_v values. Without the inversion, the effects of the spread in ϵ_v values and the spread in X_0 values remain intertwined in producing a spread in S_c values.

2. Sampling site and schedule

The sampling site is on the University of Missouri–Rolla campus, located in Rolla, Missouri. Rolla is a largely nonindustrial town, with a population of 13 500. The closest large cities are St. Louis, located 167 Km to the northeast, and Springfield, located 180 Km to the southwest. An earlier air sampling program at the same site (Alofs and Liu 1981) showed that CCN concentrations correlated only very weakly with wind direction, which suggests that the site is reasonably free of local pollution sources. Concentrations of CCN were considerably higher than continental averages, however, indicating that the site is situated within a CCN source region of perhaps synoptic scale (1000 Km). A sampling duct brought 300 L min^{-1} of outside air into a first floor room of a four story building, wherein the instrumentation was located. Further details on the site and the sampling duct are given in the earlier report (Alofs and Liu 1981).

Sampling was performed nearly 24 hours per day. Data which accumulated during the daytime working hours was processed as a single set for each day. Such a dataset is called "daily daytime," and typically represents a time period from 0800 to 1630 UTC. The equipment also ran unattended overnight, and the data which accumulated between the hours 1700 to 0730 UTC of the next day is therefore called "daily overnight." Each of the daily datasets is for a particular size setting of the EAC. The number of daily daytime datasets are 29, 32, and 21, for EAC size settings of 0.2, 0.3, and 0.4 μm diameter, respectively. The corresponding number of daily overnight datasets are 39, 34, and 30, respectively. The datasets are quite uniformly distributed throughout the four seasons of the year. Most of the data was taken during 1985, but a small portion of the total dataset was taken during 1982 and 1983.

3. Apparatus

A flow of 1.5 L min^{-1} passes from the sampling duct into a so-called diffusion dryer—the purpose of the dryer is to greatly reduce the relative humidity, so that the aerosol particles will be at their dry size when they pass out of the diffusion dryer and into the EAC. The diffusion dryer consists of cylindrical layers, the outermost being a casing, to withstand the slightly negative

FIG. 1. Presentation of Hänel's computed values of critical supersaturations.

line pressure without leaking, the next layer being granules of a desiccant material, and the innermost layer being a metal screen, to hold the desiccant in place. The aerosol sample flows through the tube formed by the screen; thus by molecular diffusion, water vapor passes from the aerosol into the desiccant material. The length and diameter of the cylindrical screen is 60 cm by 1.2 cm, respectively.

The entire flow from the diffusion dryer passes into an electrostatic aerosol classifier (EAC) of the type described by Liu and Pui (1974). The EAC is a TSI model 3071 (TSI Inc., 500 Cardigan Road, St. Paul, MN 55164, USA). The EAC delivers 1.5 L min^{-1} of size classified aerosol. A 6.0 L min^{-1} flow of filtered room air also flows into the EAC. Due to room air conditioning, the relative humidity of this air is always less than 50%, which is sufficiently low that the particles remain dry while within the EAC. The flows into and out of the EAC are such that the electrical mobilities of the particles coming out of the EAC have a spread of plus and minus 25% of the mobility at the peak of the EAC transfer function. Particles carrying one electrical charge have dry diameters in the ranges 0.173–0.243, 0.256–0.371, and 0.338–0.500 μm for classifier settings of 0.2, 0.3, and 0.4 μm, respectively. Particles carrying more than one electrical charge are larger and generally less numerous than the singly charged particles. The EAC is capable of higher size resolution than used here, but higher size resolution would have given lower particle counts. Even with this low size resolution sampling times of 8 hours were required to get good sample statistics.

The University of Missouri–Rolla isothermal haze chamber (Alofs and Trueblood 1981) is used to measure the spectra of S_c for the particles passing out of the EAC. This haze chamber consists of two vertical plates 100 cm long in the vertical direction and 13 cm wide, with a 0.8 cm spacing between the plates. The air sample flows downward between the plates in a small diameter stream surrounded by filtered air. The sample flow rate is 0.008 L min^{-1} and the filtered air flow rate is 1.0 L min^{-1} for an EAC setting of 0.2 μm, and 0.35 L min^{-1} for a setting of 0.3 μm or 0.4 μm. Both plates have a temperature of 25 C, and have wet filter paper on the surfaces.

The air sample is thus humidified to 100% relative humidity, and the sample particles swell to form haze drops. The residence time in the haze chamber is sufficient for the haze drops to reach their equilibrium size, and the haze drops are then passed into an optical particle counter to measure the haze drop size distribution. The optical particle counter is a Climet model 201 (Climet Instruments Co., 1320 Colten Ave., Redlands, California 92374). A pulse height analyzer with 1024 channels served as a data acquisition system. The pulse height analyzer is a Nuclear Data model 220 (Nuclear Data Inc., Gulf and Meacham Roads, Schaumburg, Illinois, 60196).

4. Calibration with sodium chloride

The apparatus was calibrated on about a weekly basis using NaCl aerosol in place of the atmospheric aerosol. The NaCl aerosol was produced by atomizing aqueous NaCl solutions (Alofs et al. 1979). About ten different EAC size settings were used to cover the entire range of the haze chamber (0.01% < S_c < 0.10%). Let dn/dS denote the critical supersaturation spectrum of particles coming out of the EAC, defined such that $(dn/dS)dS$ represents the concentration of particles with S_c in the range S to $S + dS$. The dn/dS is measured with the haze chamber and typically shows a main peak due to the particles with one electrical charge and a smaller peak due to particles carrying two electrical charges. Let S_2 denote the location of the main peak; i.e., S_2 is the critical supersaturation at the maximum value of dn/dS.

The values of S_2 provide a calibration of the haze chamber (Alofs and Trueblood 1981). These values as measured are really channel numbers of the Nuclear data pulse height analyzer. The values of supersaturation corresponding to these channel numbers are obtained from the size settings of the EAC and an equation relating size to critical supersaturation for NaCl. The equation used is $S_c X_0^{3/2} = 0.003327$, with S_c in % and X_0 in μm. The constant in this equation was obtained in the same way as (5) was obtained, that is, the values from Table X in Hänel (1976) were utilized.

Fitzgerald et al. (1981) summarized the performance of the isothermal haze chambers tested at the Third International Cloud Condensation Nuclei Workshop. They state ". . . the UMR IHC does show good number concentration agreement with the NRL mobility analyzer as well as better agreement with the theoretical S_c's in the monodisperse experiments. This is understandable since the UMR chamber was essentially calibrated with a mobility classifier, which may be a better method for applied CCN counting." Thus the performance of the UMR haze chamber, when calibrated in the way described in this section, has been verified by blind experiments at an international workshop.

5. Presentation of the merged data

In order to study the fundamental trends in the data as a function of EAC size setting, all of the data for each EAC setting was combined to form a "merged dataset" to represent that EAC setting. To form the merged dataset equal weight was given to each daily dataset. Thus each measured supersaturation spectra, dn/dS, was normalized with respect to the number of particles in that spectra; then all the normalized spectra for a particular EAC setting were added together, and then again normalized. The resulting dataset is shown in Fig. 2. The total number of particles in this set are 67 million, 26 million, and 7 million, at classifier settings of 0.2, 0.3, and 0.4 μm diameter, respectively.
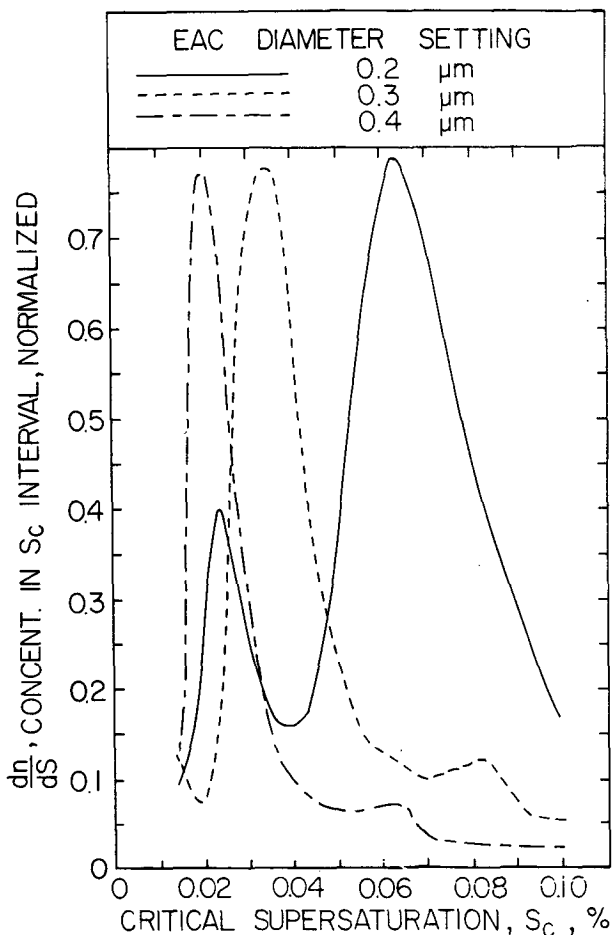
FIG. 2. The merged dataset; differential supersaturation spectra downstream of the electrical aerosol classifier (EAC).

The curve for 0.2 μm (Fig. 2) shows two peaks; the larger peak is due to the more numerous singly charged particles, the smaller peak (at lower S_c) is due to the larger particles carrying two electrical charges. The curves for 0.3 and 0.4 μm do not show a peak for doubly charged particles because the lower S_c limit of the data is too high. The values of S_2 (location of main peak) are 0.063%, 0.034%, and 0.020% at EAC setting of 0.2, 0.3, and 0.4 μm, respectively. If these pairs of critical supersaturation and dry size are used in (5), the indicated ϵ_v values are 0.71, 0.71, and 0.85, respectively. The more rigorous inversion method will indicate mean ϵ_v values of about 0.5 for all three EAC size settings; thus this simple method of obtaining mean ϵ_v values consistently overestimates ϵ_v.

6. Applying the Fitzgerald et al. simple method

The dn/dS curves seen in Fig. 2 have been numerically integrated to obtain the cumulative supersaturation spectra shown in Fig. 3. The lower integration limit is set to avoid doubly charged particles, and

equals 0.037%, 0.018%, and 0.01% for 0.2, 0.3, and 0.4 μm data respectively. Fitzgerald et al. (1982) define a mean S_c in terms of the values of S_c where the cumulative supersaturation spectrum has reached 10% and 90% of the peak value. Let these be denoted S_{10} and S_{90}. They are indicated in Fig. 3 by the circles. Also let S_F denote the Fitzgerald et al. mean S_c, defined by the relation 2 $\log(S_F) = \log(S_{10}) + \log(S_{90})$. The spectra in Fig. 3 yield S_F values of 0.065%, 0.045%, and 0.032%. Let X_F denote the Fitzgerald et al. mean dry size, defined by 2 $\log(X_F) = \log(X_{min}) + \log(X_{max})$, where X_{min} and X_{max} are the minimum and maximum diameter of singly charged particles transmitted by the EAC. The values of X_F are 0.2050, 0.3082, and 0.4111 μm. When the three pairs of S_F, X_F values are put into (5), the resulting ϵ_v values are 0.62, 0.38, and 0.31 for EAC settings of 0.2, 0.3, and 0.4 μm, respectively.

The Fitzgerald et al. method can be applied in a second way to give values of ϵ_v near 0.55 for all three EAC settings. This second way requires adjusting the upper S_c boundary of the data as follows: For 0.4 μm and 0.3 μm EAC settings, data for S_c larger than 0.04% and 0.06%, respectively, are neglected. For 0.2 μm EAC setting, the upper S_c limit is moved to 0.11%, which requires a slight extrapolation of the dn/dS curve (Fig. 2). The second way of applying the Fitzgerald et al. method is not as arbitrary as it might at first seem. The guiding principle is to use only data comprising the main peak on the dn/dS curve for a given EAC setting. As discussed below, the inversion method presented in this paper gives erratic results unless the S_c region is likewise restricted to that including only the main peak in dn/dS.
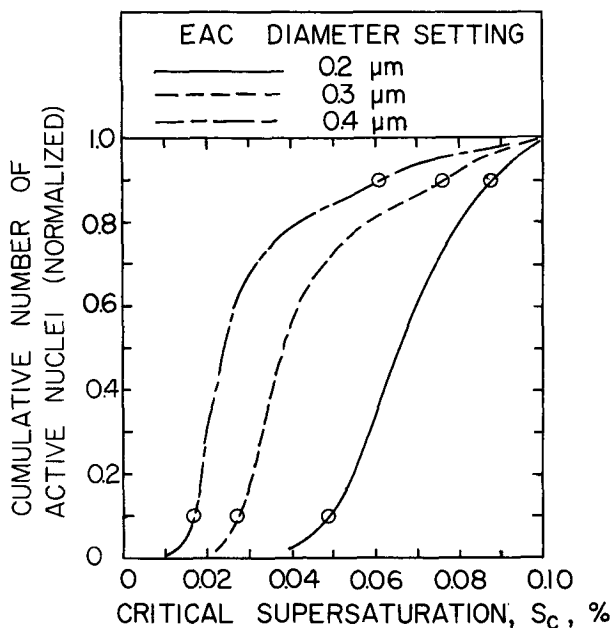

FIG. 3. The merged dataset; cumulative supersaturation spectra for the singly charged particles.

7. Formulation of the inversion problem

Let X, S, and ϵ be abbreviations for X_0, S_c, and ϵ_v, respectively. Let dN/dX denote the dry particle size distribution, at the inlet of the EAC, such that the number of particles with dry diameter in the range X to $X + dX$ is $(dN/dX)dX$. Let the transfer function for the EAC be denoted $G(v, X)$, defined to be the fraction of particles at the EAC inlet which pass out of the EAC. Here v denotes the voltage of the EAC, and for this investigation, v takes on only three different values, corresponding to the three different size settings used (0.2, 0.3, and 0.4 μm). When performing a particular inversion, v is a constant. The paper by Hagen and Alofs (1983) gives expressions for $G(v, X)$, and the reader is referred to the appendix of that paper for the details.

Let the probability distribution for ϵ be denoted by P, and assume P depends only on ϵ. Then the probability that a given particle has a volume fraction of soluble material in the range ϵ to $\epsilon + d\epsilon$ is $Pd\epsilon$. The number of particles at the EAC output in the size range X_1 to X_2 and in the ϵ range ϵ_1 to ϵ_2 is given by the following double integral:

$$\int_{X_1}^{X_2} \int_{\epsilon_1}^{\epsilon_2} (dN/dX)G(v, X)Pd Xd\epsilon. \qquad (7)$$

Now consider the same integrand as in the above integral, but let the integration be performed over a region of X, ϵ space such that the particles have critical supersaturation in the range S to $S + dS$. This region is shown in Fig. 4, with the top of the region bounded by a line in X, ϵ space such that critical supersaturation is constant at a value S, and with the bottom of the region bounded by a line such that critical supersaturation equals $S + dS$. The integration region is bounded on the left and right by the X values (X_1 and X_2). The top line in Fig. 4 defines ϵ as a function of X, call this function $\epsilon_2(X)$. The bottom line defines a different function, call it $\epsilon_1(X)$. The functions ϵ_1 and ϵ_2 are obtained from (5) evaluated at $S + dS$, or at S, respectively. Then the double integral over the region in X, ϵ space such that critical supersaturations lie in the range S to $S + dS$ is represented by the following iterated integral (Kaplan 1952, page 193):

$$\int_{X_1}^{X_2} \left\{ \int_{\epsilon_1(X)}^{\epsilon_2(X)} (dN/dX)G(v, X)P[\epsilon(X, S)]d\epsilon \right\} dX. \qquad (8)$$

The upper limit of integration on the above inner integral is only slightly larger than the lower limit of integration, because dS is a differential quantity. Thus we may write:

$$\epsilon_2(X) = \epsilon_1(X) + \frac{\partial \epsilon}{\partial S} dS, \qquad (9)$$

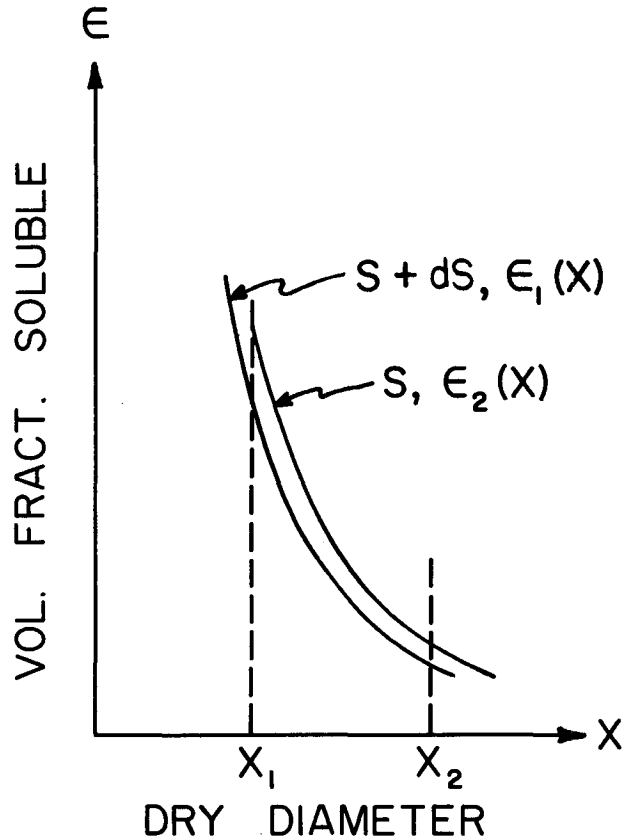where $\dfrac{\partial \epsilon}{\partial S}$ is obtained analytically from (5) and thus is

FIG. 4. Region of integration in X, ϵ space so as to include only particles with critical supersaturation between S and $S + dS$.

a known function of S and X. Thus the inner integral in (8) reduces to:

$$\left(\frac{\partial \epsilon}{\partial S}\right)dS\left(\frac{dN}{dX}\right)G(v, X)P[\epsilon(X, S)]. \qquad (10)$$

Hence (8) reduces to the single integral

$$\int_{X_1}^{X_2} \left(\frac{dN}{dX}\right)G(v, X)P[\epsilon(X, S)]\left[\frac{\partial \epsilon}{\partial S}\right]dXdS. \qquad (11)$$

The number of particles at the EAC output with critical supersaturations in the range S to $S + dS$ is given by either (11) or by $(dn/dS)dS$, where dn/dS has already been defined to be the supersaturation spectrum measured by the haze chamber. Thus the governing equation describing the inversion is

$$\frac{dn}{dS} = \int_{X_1}^{X_2} \left(\frac{dN}{dX}\right)G(v, X)P[\epsilon(X, S)]\left[\frac{\partial \epsilon}{\partial S}\right]dX. \qquad (12)$$

The range of integration in (12) needs to be sufficiently large to include particles carrying single and double electrical charges, because as seen in Fig. 1, the doubly charged particles contribute a second peak. There is no difficulty however in making the range of

integration large enough to include particles with more than two charges.

Size distributions, dN/dX, were not measured in this investigation. Numerical calculations described later in this paper indicate that inversion results are quite insensitive to dN/dX. For now, it suffices to say that the final calculations are done using Whitby's "grand average continental" size distribution (specified in Table 2 of Whitby 1978).

8. The inversion algorithm

The inversion problem is to obtain P in (12). We wish to replace (12) by a set of linear algebraic equations. To this end, we will determine P at only a finite number of ϵ values. Let ϵ_k denote these values, with $k = 1, 2, 3 \cdots K$. Usually K is 12. Also let P_k be the corresponding P values. Thus the P_k are the unknowns to be determined by the inversion algorithm. The measured supersaturation spectrum is represented by a finite number of S_i values, $i = 1, 2, 3 \cdots I$ and corresponding dn/dS values. Usually I is in the range 20 to 40. The continuous size range corresponding to the lower (X_1) and upper (X_2) integration limits in (12) is represented by J discrete sizes, denoted $X_j, j = 1, 2, 3 \cdots J$. Usually J equals 600. Thus, the width of the size step (w) equals $(X_2 - X_1)/(J - 1)$.

For a given S_i and X_j, (5) defines a value of ϵ, call it $\epsilon_{i,j}$. Let the ϵ_k closest to $\epsilon_{i,j}$ be called ϵ_p, thus defining p to be a particular value of k. A three point interpolation is used to approximate $P(\epsilon)$ near ϵ_p,

$$P_p(\epsilon) = Z_{p_2}\epsilon^2 + Z_{p_1}\epsilon + Z_{p_0}.$$

The Z's depend on $\epsilon_{p-1}, \epsilon_p, \epsilon_{p+1}, P_{p-1}, P_p$, and P_{p+1}. The expression $P_p(\epsilon)$ is linear in the P's. It is useful to algebraically rewrite the expression in the form

$$P_p(\epsilon) = \sum_q Q(q, \epsilon)P_q; \quad q = p - 1, p, p + 1.$$

Here $Q(q, \epsilon)$ is found to be a quadratic polynomial in ϵ, i.e.,

$$Q(q, \epsilon) = U_{q_2}\epsilon^2 + U_{q_1}\epsilon + U_{q_0}.$$

The U's are known functions of $\epsilon_{p-1}, \epsilon_p$, and ϵ_{p+1}. They do not depend on the P's. Using this interpolation scheme, P at ϵ_{ij} may be written:

$$P_{ij} = \sum_q (Q_{i,j,q})(P_q); \quad q = p - 1, p, p + 1, \quad (13)$$

where $Q_{i,j,q} = Q(q, \epsilon_{ij})$. It is important to note that Q's are not unknowns. Instead they are known functions, quadratic in ϵ, which allow P_{ij} to be expressed in terms of the unknown P_q's via interpolation.

The following set of I linear algebraic equations thus replaces (12):

$$\left(\frac{dn}{dS}\right)_i = \sum_{j=1}^J T_j(\partial\epsilon/\partial S)_{ij} \sum_q Q_{ijq}P_q, \quad (14)$$

where $T_j = w\beta_j(dN/dX)_jG(v, X_j)$, and where $\beta_j = 0.5$ for $j = 1$ or for $j = J$; otherwise $\beta_j = 1.0$. A given unknown, P_k, will appear multiple times in the summation in (13). The equation can be rewritten in a form in which each unknown appears only once:

$$\left(\frac{dn}{dS}\right)_i = \sum_{k=1}^K Z_{ik}P_k \quad (15)$$

where

$$Z_{ik} = \sum_{j=1}^J T_j(\partial\epsilon/\partial S)_{ij} \sum_{q=p-1}^{p+1} Q_{ijq}\delta_{kq} \quad (16)$$

and $\delta_{kq} = (0$ if $k \neq q$, 1 if $k = q)$. The P_k are determined by using a canned program for minimizing $\|dn/dS - ZP\|$ subject to the constraint $P_k \geq 0$. Physically, the P_k need to be positive or zero.

9. Applying the inversion to the merged data

When the inversion algorithm is applied to the merged data for the entire experimental S_c range, the results are erratic; i.e., the P values do not correlate with the ϵ values, for any of the three EAC settings. However, if the S_c range for a particular EAC setting is restricted to include only the primary peak in dn/dS, the P values do correlate with the ϵ values, as can be seen in Fig. 5.
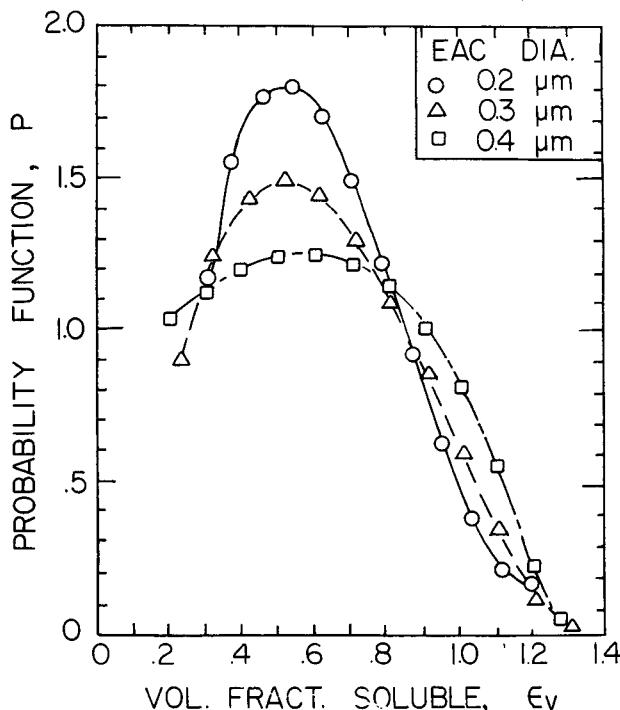

FIG. 5. Results of the inversion for S_c range restricted to region of main dn/dS peak.

The circles, triangles and squares in Fig. 5 are the individual P, ϵ pairs ($K = 12$) from the inversions for EAC settings of 0.2, 0.3, and 0.4 μm, respectively. The input data to the inversions are shown in Fig. 6 by circles, triangles and squares. Note from Fig. 6 that the input data covers only a restricted S_c range in the vicinity of the main dn/dS peak for a particular EAC setting. A comparison of Fig. 6 with Fig. 2 will show what data has been left out in Fig. 6.

The three continuous curves in Fig. 6 are the result of three numerical "forward" integrations of (12), using three $P(\epsilon)$ functions represented by the three curves in Fig. 5. Figure 6 indicates that the forward integration of the inversion output gives nearly the same dn/dS as the input data to the inversion algorithm, which lends confidence that the inversion has performed satisfactorily for these limited S_c ranges.

Consider next the question of why the inversion does not give physically reasonable $P(\epsilon)$ when data for the entire S_c range is provided as input. For the case of the 0.4 μm EAC setting, the dn/dS data shows a small peak at $S_c = 0.064\%$. (See Fig. 2, dot-dash curve.) This might be due to singly charged particles having smaller ϵ than those causing the primary peak. If so, one would expect a bimodal $P(\epsilon)$, with a main peak like the dot-dash

curve in Fig. 5, and a smaller peak at smaller ϵ, probably at about $\epsilon = 0.06$, estimated from (5) at $S_c = 0.064\%$ and $X_0 = 0.4$ μm. Similar comments apply to the small peak seen at $S_c = 0.083\%$ for EAC setting of 0.3 μm. (See Fig. 2, dotted curve.)

Recall that usually only 12 values of $P(\epsilon_k)$ are obtained from the inversion, and the ϵ_k are specified as input to the inversion. Thus the range of ϵ is specified before starting the inversion algorithm. Note that the ϵ range in Fig. 5 is approximately 0.2 to 1.3. Experience shows that if the number of ϵ points is increased very much above 12, or if the spacing between the ϵ points gets too large, the inversion gives erratic results. There appears to be some sort of stability problem when the inversion is applied to a large ϵ range.

In summary, the data (Fig. 2) suggest bimodal $P(\epsilon)$, with a main peak at $\epsilon = 0.5$, and a smaller peak at $\epsilon < 0.1$, but the inversion failed to indicate the smaller peak, because the inversion was unstable when run for a sufficiently large ϵ range to allow the expected bimodal $P(\epsilon)$.

There is another sense in which the inversion is only partly successful. An assumption in the inversion is that the probability distribution for ϵ is independent of particle size. If this assumption is true, all three EAC size settings would, ideally, give the same $P(\epsilon)$. The $P(\epsilon)$ in Fig. 5 all have a maximum near $\epsilon = 0.5$, but they suggest that smaller particles have less spread in ϵ.

Let σ denote the standard deviation in ϵ, based on representing the $P(\epsilon)$ in Fig. 5 by Gaussian distributions:

$$P = E_1 \exp - (\epsilon - 0.5)^2/2\sigma^2, \qquad (17)$$

where E_1 is the normalization constant. The σ values obtained by fitting the curves in Fig. 5 to (17) are 0.292, 0.361, and 0.549 at EAC settings of 0.2, 0.3, and 0.4 μm, respectively. These σ values are plotted as a circle, triangle, and square in Fig. 7. Various possible assumed linear variations of σ with X are shown by the straight lines in Fig. 7.

Figure 8 shows the results of six forward integrations of (12), using $P(\epsilon, X)$ as specified by (17) for $\epsilon > 0.2$, and with $P(\epsilon, X) = 0$ for $\epsilon < 0.2$. Fig. 8 is with σ varying either linearly with X, or held constant. The cases where σ varies linearly with X give the lines in Fig. 8, the cases where σ is constant give the symbols. The style of line or symbol in Fig. 8 corresponds to the assumed σ variation indicated in Fig. 7.

Since the lines in Fig. 8 lie close to the corresponding symbols at a particular EAC setting, it appears that neglecting the X dependence of $P(\epsilon, X)$ in the inversion is not a serious oversimplification. If so, the inversion indicates that in the ϵ range 0.2 to 1.3, the ϵ probability distribution is approximately Gaussian, with a peak near $\epsilon = 0.5$, and a σ which increases with particle size.

An alternative interpretation, is that the three $P(\epsilon)$ curves in Fig. 5 are identical, within the error limits of

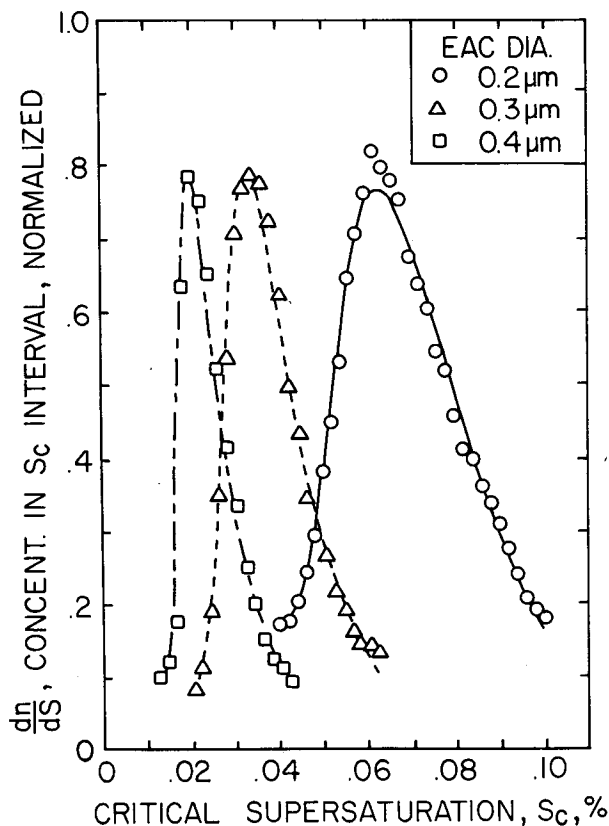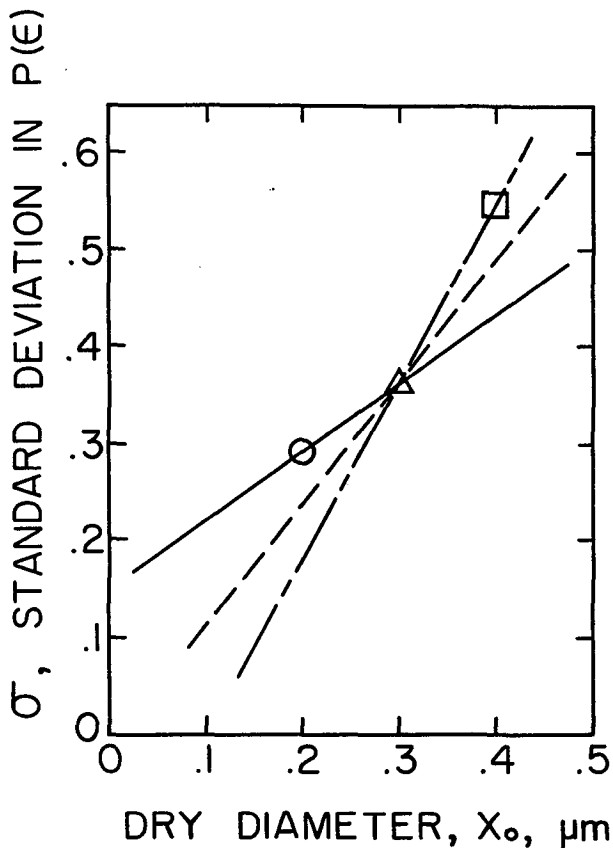FIG. 6. Data used as input to the inversions (squares or triangles), and results for forward integration (curves) of the inversion outputs.

FIG. 7. Symbols (circle, square, triangle) denote σ values obtained by fitting equation 17 to $P(\epsilon)$ curves shown in Fig. 5. Lines show three assumed variations of σ with X.

the experiments. These error limits are not known. With this interpretation, σ is independent of particle size for the size range of this investigation.

The former interpretation would require 0.4 μm diameter particles to have a more variable chemical composition than 0.2 μm particles, and this does not appear likely in terms of current knowledge of how particles in this size range are formed and removed.

10. Effect of size distribution

Since the size distribution of the atmospheric aerosol was assumed rather than measured, there is a need to investigate the sensitivity of the experiment to the assumed size distribution. Whitby's "urban average" size distribution (case 6 in Table 1 of Whitby 1978) is quite different from his "grand average continental" (Table 2 from Whitby 1978). Forward integrations of (12) using these two size distributions gave supersaturation spectra (dn/dS functions) which agreed very closely. The agreement was better than the agreement seen in Fig. 8. Thus we conclude that only a small error is introduced by assuming that the size distribution is equal to the Whitby grand average continental.

11. Presentation of the daily datasets

The S_2 has already been defined as the S_c where dn/dS has the highest maximum. Let S_1 and S_3 be defined to be the S_c where dn/dS equals 61% of this maximum dn/dS. Then $S_3 - S_1$ is a measure of the width of the main peak in dn/dS. Figure 9 presents values of S_1, S_2, and S_3 for the daily datasets. The circles show the values of S_2, and the horizontal bar end points represent values of S_1 and S_3. The date for each data point is also shown, and the label at the top of the columns indicates the EAC size setting, and whether the data was taken during the day or overnight.

It can be seen from Fig. 9 that there is a large day to day variation, both in peak location (S_2) and in the peak width ($S_3 - S_1$). This justifies the need for a long-term sampling program, such as this one, if one wants reliable average conditions.

Table 1 gives a simple statistical analysis of the data in Fig. 9. The relative standard deviation in Table 1 is
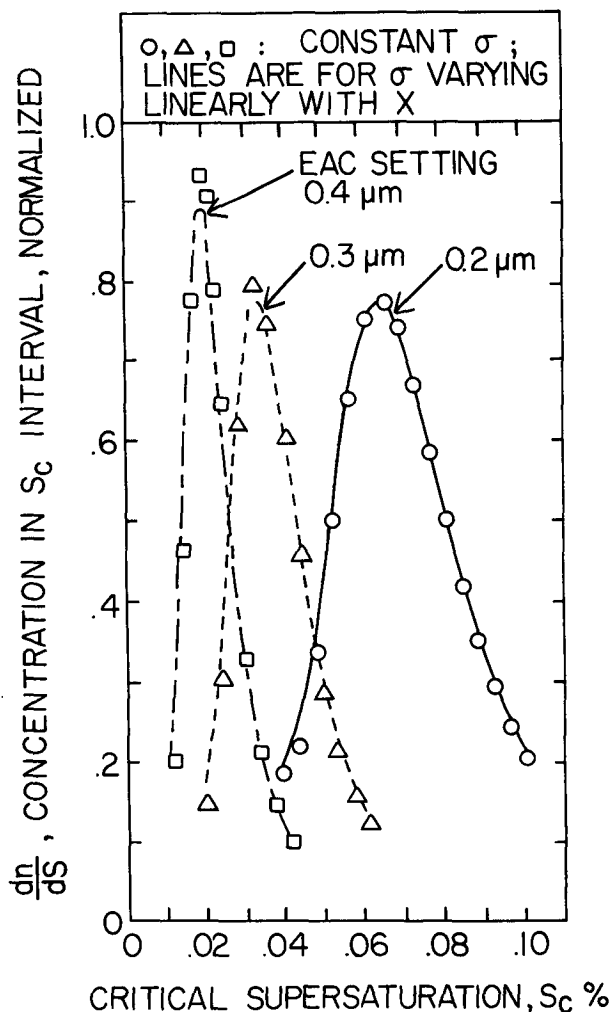

FIG. 8. The effect of assuming σ values or variations as shown in Fig. 7 by the corresponding symbol style or line style.
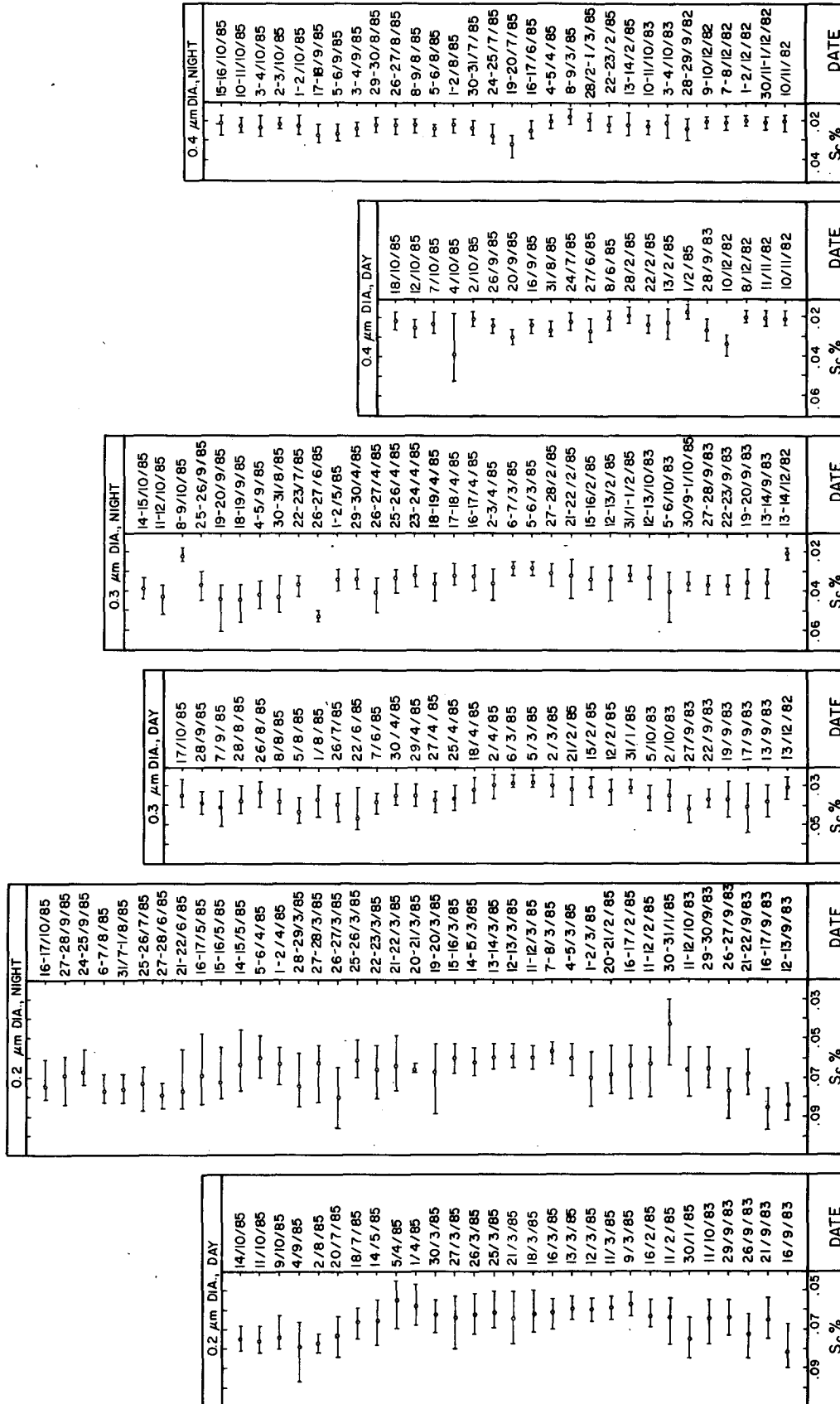
FIG. 9. Presentation of daily datasets. Circles show location of main peak in dn/dS. Bars show width of main peak at 61% of peak height.

TABLE 1. Statistics for daily datasets.

Type of daily data	Mean (%)		Relative std. dev.	
	S_2	$(S_3 - S_1)/2$	S_2	$(S_3 - S_1)/2$
0.2 μm day	.0662	.0095	.109	.279
0.2 μm night	.0675	.0110	.123	.341
0.3 μm day	.0349	.0066	.215	.295
0.3 μm night	.0357	.0065	.176	.374
0.4 μm day	.0243	.0050	.206	.590
0.4 μm night	.0228	.0041	.122	.232

the standard deviation of that quantity, divided by the mean of that quantity. It can be seen from Table 1 that there are not systematic differences between the daytime data and the overnight data. This lack of a diurnal pattern is surprising because of the many known roles of solar radiation in gas to particle conversion processes. The size range of this investigation corresponds to the accumulation range (Whitby 1978), which is at least indirectly formed by gas to particle processes.

12. Comparison to other investigations

The mean value of the apparent volume fraction of soluble material (ϵ_v) from this study is about 0.5. This value is now compared to the results of other investigations reported in the literature. In many cases a different parameter than ϵ_v is reported, so approximate conversions to ϵ_v values are made.

Meszaros (1968) made ground level measurements near Budapest, Hungary, collecting aerosol particles on filters and then developing the filters in a humidity chamber. He reports that the mass fraction of water soluble material varied with particle diameter (X_0) as follows: 0.17 for $X_0 < 0.28$ μm, and 0.075 for $X_0 > 0.28$ μm.

Laktionov (1972) reports that the mass fraction of water soluble material is about 0.2 for $X_0 = 0.3$ μm and is about 0.1 for $X_0 = 0.6$ μm. Laktionov does not report for how many days data were taken. His measurements were made from an airplane, at altitudes of 100 to 5000 m flying over 3 different geographic regions in the USSR.

Winkler (1973) reports that the mass fraction of water soluble materials is about 0.6 for particles larger than 0.2 μm diameter. The particles were collected near Mainz, West Germany and were analyzed using the gravimetric technique described by Winkler and Junge (1972).

Hänel and Lehmann (1981), collected particles in a large size range whose lower limit varied between 0.14 and 2 μm diameter and whose upper limit varied between 2 and 20 μm. The particles were analyzed using an improved Winkler and Junge (1972) gravimetric method. The mass fraction of water soluble material was determined, and ranged from 0.31 to 0.89, de-

pending on the geographic location and the lower and upper limits of the size range collected.

If one makes the crude assumption that the mass fraction of water soluble material equals ϵ_v, the first two investigations cited above give lower ϵ_v than the present investigation, and the last two give roughly the same ϵ_v as the present investigation.

Fitzgerald et al. (1982) report values of B_c, which we convert to values of ϵ_v using the relation $\epsilon_v = 1.587 B_c$. For measurements in the Washington, D.C. area performed during a 3-day period, the mean ϵ_v value is 0.36. Similar measurements by Fitzgerald and Hoppel (1984) were made in various geographic regions on 11 different days between 1978 and 1980. These give a mean ϵ_v of 0.46. The particle diameter range for both the above studies is about 0.04 to 0.1 μm, and thus represents smaller particles than the present investigation.

Sekigawa (1983) reports ϵ_v values measured in Japan for the size range 0.05 to 0.2 μm diameter. Data taken during several days of one month differed considerably from those taken during a different month, but the mean value of ϵ_v is about 0.5. The data indicated that ϵ_v increases as particle size increases.

The observed mean ϵ_v value of 0.5 for the present investigation is within the range of scatter shown by the other investigations we have just reviewed. Our finding that the mean ϵ_v value does not vary with particle size does not agree with the result of Meszaros (1968) or of Laktionov (1972), who found ϵ_v decreases as particle size increases, while Sekigawa (1983) reports the opposite trend with particle size.

13. Summary

Atmospheric aerosol particles were passed through an electrostatic aerosol classifier (EAC) and then through an isothermal haze chamber. The EAC passes particles in a rather narrow range of dry diameter (X_0). The haze chamber is used to measure the spectra of critical supersaturations (S_c) of these size classified particles.

The data were obtained 24 hours per day, for about 100 days, at one location (Rolla, Missouri). The day to day variations in S_c spectra were very large. Data taken from 0800 to 1630 UTC exhibited nearly the same average S_c spectra as that taken during the period 1700 to 0730 UTC.

The S_c spectra are inverted to obtain spectra of ϵ_v, the apparent volume fraction of water soluble material, defined such that for particles composed only of ammonium sulfate and water insoluble compounds, ϵ_v is the volume fraction of ammonium sulfate. The inversion algorithm, which is presented for the first time in this paper, indicates that the probability distribution for ϵ_v is approximately Gaussian over the ϵ_v range 0.2 to 1.3. The peak in the ϵ_v distributions is at $\epsilon_v = 0.5$ for EAC diameter settings of 0.2, 0.3, and 0.4 μm. The

inversion algorithm showed two shortcomings. First, an assumption in the inversion is that the probability distribution for ϵ_v is independent of particle size, but the width of the ϵ_v distributions increased as the EAC diameter setting increased. Second, the spectra of S_c suggest bimodal ϵ_v spectra, with a secondary peak for $\epsilon_v < 0.1$. The inversion did not indicate the secondary peak in the ϵ_v distributions, because the inversion was unstable when run over the complete S_c range corresponding to $\epsilon_v < 0.1$.

REFERENCES

Alofs, D. J., and T. H. Liu, 1981: Atmospheric measurements of CCN in the supersaturation range 0.013%–0.681%. *J. Atmos. Sci.,* **38,** 2772–2778.

——, and M. B. Trueblood, 1981: UMR dual mode CCN counter. *J. Rech. Atmos.,* **15,** 219–223.

——, ——, D. R. White and V. L. Behr, 1979: Nucleation experiments with monodisperse NaCl aerosols. *J. Appl. Meteor.,* **18,** 1106–1117.

Fitzgerald, J. W., and W. A. Hoppel, 1984: Equilibrium size of atmospheric aerosol particles as a function of relative humidity: Calculations based on measured aerosol properties. *Hygroscopic Aerosols,* L. H. Ruhnke and A. Deepak, Eds., Spectrum Press, 21–33.

——, —— and M. Vietti, 1982: The size and scattering coefficient of urban aerosol particles at Washington DC as a function of relative humidity. *J. Atmos. Sci.,* **39,** 1838–1852.

——, C. F. Rogers and J. G. Hudson, 1981: Review of isothermal haze chamber performance. *J. Rech. Atmos.,* **15,** 333–346.

Hagen, D. E., and D. J. Alofs, 1983: Linear inversion method to obtain aerosol size distributions from measurements with a differential mobility analyzer. *Aerosol Sci. Tech.,* **2,** 465–475.

Hänel, G., 1976: The properties of atmospheric aerosol particles as functions of the relative humidity at thermodynamic equilibrium with the surrounding moist air. *Adv. Geophys.,* **19,** 73–188.

——, and M. Lehmann, 1981: Equilibrium size of aerosol particles and relative humidity: New experimental data from various aerosol types and their treatment for cloud physics application. *Contrib. Atmos. Phys.,* **54,** 57–71.

Kaplan, W., 1952: *Advanced Calculus.* Addison-Wesley, 679 pp.

Laktionov, A. G., 1972: The concentration of water-soluble substances in atmospheric aerosol particles. *Atmos. Oceanic Phys.,* **8,** 221–224.

Liu, B. Y. H., and D. Y. H. Pui, 1974: A submicron aerosol standard and the primary, absolute calibration of the condensation nuclei counter. *J. Colloid Interface Sci.,* **47,** 155–171.

Meszaros, E., 1968: On the size distribution of water soluble particles in the atmosphere. *Tellus,* **20,** 443–448.

Sekigawa, K., 1983: Estimation of the volume fraction of water soluble material in submicron aerosols in the atmosphere. *J. Meteor. Soc. Japan,* **61,** 359–366.

Whitby, K. T., 1978: The physical characteristics of sulfur aerosols. *Atmos. Environ.,* **12,** 135–159.

Winkler, P., 1973: The growth of atmospheric aerosol particles as a function of the relative humidity—Part II: An improved concept of mixed nuclei. *Aerosol Sci.,* **4,** 373–387.

——, and C. Junge, 1972: The growth of atmospheric aerosol particles as a function of the relative humidity—Part I: Method and measurements at different locations. *J. Rech. Atmos.* (Memorial Henri Dessens.)